Crustal domains in the Western Barents Sea

Alexey Shulgin [1], Jan Inge Faleide,[1] Rolf Mjelde,[2] Asbjørn Breivik[1] and
Ritske Huismans[2]

[1]*Centre for Earth Evolution and Dynamics (CEED), University of Oslo, 0372 Oslo, Norway. E-mail: alexey.shulgin@geo.uio.no.*
[2]*Department of Earth Science, University of Bergen, 5007 Bergen, Norway*

SUMMARY

The crustal architecture of the Barents Sea is still enigmatic due to complex evolution during the Timanian and Caledonian orogeny events, further complicated by several rifting episodes. In this study we present the new results on the crustal structure of the Caledonian–Timanian transition zone in the western Barents. We extend the work of Aarseth *et al. (2017)*, by utilizing the seismic tomography approach to model Vp, Vs and Vp/Vs ratio, combined with the reprocessed seismic reflection line, and further complemented with gravity modelling. Based on our models we document in 3-D the position of the Caledonian nappes in the western Barents Sea. We find that the Caledonian domain is characterized by high crustal reflectivity, caused by strong deformation and/or emplacement of mafic intrusions within the crystalline crust. The Timanian domain shows semi-transparent crust with little internal reflectivity, suggesting less deformation. We find, that the eastern branch of the earlier proposed Caledonian suture, cannot be associated with the Caledonian event, but can rather be a relict from the Timanian terrane assemblance, marking one of the crustal microblocks. This crustal block may have an E–W striking southern boundary, along which the Caledonian nappes were offset. A high-velocity/density crustal body, adjacent to the Caledonian–Timanian contact zone, is interpreted as a zone of metamorphosed rocks based on the comparison with global compilations. The orientation of this body correlates with regional gravity maxima zone. Two scenarios for the origin of the body are proposed: mafic emplacement during the Timanian assembly, or massive mafic intrusions associated with the Devonian extension.

Key words: Arctic region; seismic tomography; Crustal structure.

1 INTRODUCTION

The crustal architecture of the NW Barents Sea, NE Atlantic, is still not fully understood. The region is located in a tectonically complex area. The major part of the Eastern Barents Sea is underlain by Timanian basement (Ediacaran age), while the western Barents Sea is located on Caledonian basement, associated with the Caledonian orogeny in the Late Silurian–Early Devonian. The spatial westward extent of the Timanian domain is still an open question, which we will return to in the discussion. In 2014, a NW–SE striking wide-angle OBS profile was obtained in the western Barents Sea (Aarseth *et al.* 2017), crossing the proposed transition from the Caledonian to Timanian domains (Fig. 1). In this study, we extend the analysis of the seismic data of Aarseth *et al.* (2017) using the *P* and *S* waves tomographic approach, combined with gravity modelling and reprocessing of the collocated reflection data IKU-H (Gudlaugsson *et al.* 1987; Ritzmann & Faleide 2007). The modelling of the wide-angle seismic data (Aarseth *et al.* 2017) utilized only part of the available Vp data (and not performing any *S* modelling) and followed the forward modelling approach. Their final model also showed significant

discrepancy with the results of Ritzmann & Faleide (2007). The interpretation of the IKU-H reflection line (Ritzmann & Faleide 2007) are based on the time-to-depth conversion of the line drawing interpretation (rather than the actual depth migration of the reflection data). So the main motivation of the present study is to utilize all possible data from both data sets, processed in a combined and comparable way for joint interpretation. The main scope of this study is to clarify our understanding on the broad-scale crustal domain architecture in the NW Barents Sea and its evolution.

2 REGIONAL GEOLOGY AND TECTONICS

The evolution of the Greater Barents Sea was mainly controlled by three orogenic episodes surrounding the region: Timanian (Ediacaran: late Neoprotorozoic—early Cambrian: 560–540 Ma), Caledonian (late Silurian—Early Devonian: 430–400 Ma), Uralian (Late Carboniferous—Early Permian: 310–280 Ma; and younger orogenic activity on Novaya Zemlya and Taimyr: Late Triassic—Early Jurassic, Gee & Pease 2004; Gee *et al.* 2006; Ritzmann & Faleide
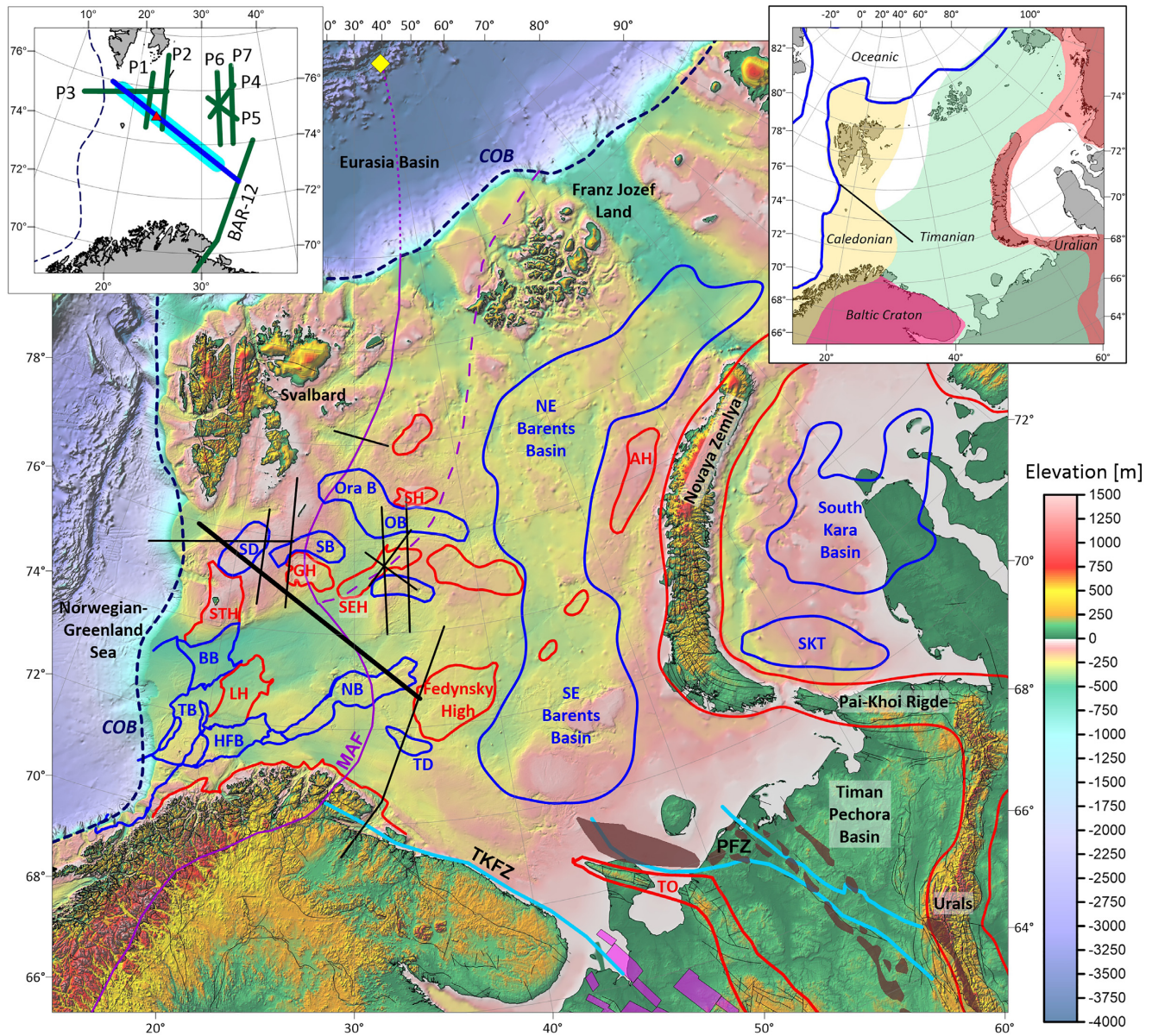
Figure 1. Hypsometric map of the Greater Barents Sea. The left insert map shows major wide-angle profiles discussed in this work. The location of the modelled profile is shown by dark blue line. Red triangle marks the OBS-227, shown on Fig. 2. Other wide-angle profiles discussed in the paper (Breivik *et al.* 2002, 2003, 2005; Shulgin *et al.* 2018) are shown by green lines. Thick cyan line shows the extent of the collocated reflection profile (IKU-H). Note the MCS line does not cover the eastern part of the wide-angle profile, due to then unsettled status of the dispute area. The right insert map shows the major tectonic provinces forming the basement of the Barents Sea (modified after Faleide *et al.* 2018). Major structural lows (blue) and highs (red) are marked (modified after Shulgin *et al.* 2018; Klitzke *et al.* 2019). The proposed eastward extent of the Caledonian basement domain is shown by purple lines (after Gernigon & Brönner 2012). Major Timanian trends are shown with light blue, EEC rifts are marked by magenta shading, extent of Devonian volcanics—brown areas (after Bogdanov & Hain 1996). The locations of the wide-angle profiles discussed in the paper are shown. Yellow diamond marks the location on the Lomonosov Ridge discussed in Knudsen *et al.* (2017). (AH)—Admiralty High; (BB)—Bjørnøya Basin; (GH)—Gardarbanken High; (HFB)—Hammerfest Basin; (LH)—Lopa High; (MAF)—Middle Allochthon Front; (NB)—Nordkapp Basin; (OB)—Olga Basin; (Ori B.)—Ori Basin; (PFZ)—pre-Pechora Fault Zone; (SB)—Sørvestsnaget Basin; (SD)—Sørkapp Depression; (SEH)—Sentralbanken High; (SH)—Storbanken High; (SKT)—South Kara Trough; (STH)—Stappen High; (TD)—Tiddlybanken Basin; (TKFZ)—Trollfjorden-Komagelva Fault Zone (TO) –Timan Orogen; (TB)—Tromsø Basin.

2007, 2009; Knudsen *et al.* 2017, Faleide *et al.* 2018, Fig. 1). The Timanides, formed as a fold-and-trust belt along the NE margin of Baltica in late Neoproterozoic–early Cambrian (Gee *et al.* 2006; Kostyuchenko *et al.* 2006). The Trollfjorden-Komagelva Fault Zone (TKFZ, Fig. 1) marks the extent of the Timanian crustal domain along the Baltic craton, stretching from the Urals to the Varanger Peninsula in northern Norway. The Timanian basement may extend even further to the west, however it is masked by the overprint of

the Caledonian orogeny, as identified from the regional geology and aeromagnetic data (Gernigon & Brönner 2012; Gernigon *et al.* 2014, 2018). The structural trends associated with the Timanides are well described onshore having a NW–SE striking direction, similar to TKFZ. The offshore continuation of these structural trends can be identified from the seismic reflection and potential field data, suggesting they continue all the way to the western Barents Sea, reaching the Tiddlybanken and Olga basins (Gernigon *et al.* 2018;

Shulgin *et al.* 2018; Klitzke *et al.* 2019; Hassaan *et al.* 2020). However, the actual western extent of the Timanian basement is still enigmatic (Roberts & Siedlecka 2002; Pease & Scott 2009).

The closure of the Iapetus Ocean in early Silurian (*ca.* 440 Ma), followed by the collision of the Laurentia and Baltica, resulted in the Caledonian orogeny, which culminated in the late Silurian to early Devonian. It affected mostly the western Barents Sea (Roberts 2003; Gee *et al.* 2006; Ritzmann & Faleide 2007; Gernigon & Brönner 2012). Based on recent interpretations of the magnetic and seismic data (Barrere *et al.* 1999, 2011; Gernigon & Brönner 2012; Gernigon *et al.* 2014, 2018) the offshore NE continuation of the Caledonian allochthon front turns NNW across the Nordkapp Basin (Fig. 1). The Caledonian deformation zone narrows around Bjørnøya, where it seems to line up with the Caledonian structures on Svalbard (Manby & Lyberis 1992; Worsley 2008). However, potential field data suggest widening of this zone northwards, between Svalbard and Franz Josef Land (Marello *et al.* 2013).

There is a long-standing debate on the geometry and eastward extent of the Caledonian crustal domain in the northern Barents Sea; whether it is represented as an individual suture or with an additional branch further east (stippled purple line on Fig. 1), originating just south of Gardarbanken High and running towards Franz Josef Land (Faleide *et al.* 1984; Doré *et al.* 1997; Gudlaugsson *et al.* 1998; Breivik *et al.* 2002, 2003, 2005; Gee *et al.* 2006; Ritzmann & Faleide 2007, 2009; Worsley 2008; Barrère *et al.* 2011; Marello *et al.* 2013; Gernigon *et al.* 2014; Aarseth *et al.* 2017; Klitzke *et al.* 2019). The dated basement sample ages change from east Svalbard to Franz Josef Land (Gee & Pease 2004; Pease 2011). Together with samples from the Lomonosov Ridge (Knudsen *et al.* 2017) they provide evidence that the Caledonian domain boundary is located somewhere between Svalbard and Franz Josef Land. The suggestion for the additional branch of the Caledonian suture, located eastwards, comes from the interpretations of the crustal velocity structure and gravity modelling (Breivik *et al.* 2002, 2003, 2005; Ritzmann & Faleide 2007; Marello *et al.* 2013; Aarseth *et al.* 2017). However, a recent seismic study in the Olga Basin (Klitzke *et al.* 2019), suggests that this suture is unlikely to exist, since it crosscuts the E–W trending Olga Basin and its associated positive gravity anomaly reflecting a continuous basement structure at depth. Or at least it was not active since the formation of the Olga Basin.

The later evolution of the Greater Barents Sea was mainly influenced by several rifting episodes. The late Devonian–early Carboniferous rifting in the Pechora Basin and eastern Barents Sea (Stoupakova *et al.* 2011) affected a major part of the eastern Barents shelf, and may also have reactivated the inherited crustal structures in the western Barents and on Svalbard. It may also have triggered mafic intrusions on the Varanger Peninsula and below the Fedynsky High (Shulgin *et al.* 2018). The Late Palaeozoic–Mesozoic rifting, associated with opening of the North Atlantic (Faleide *et al.* 1993; Johansen *et al.* 1994), dominated the evolution of the westernmost Barents shelf. In addition, Early Cretaceous magmatism associated with the High Arctic Large Igneous Province (LIP) influenced the NW part of the Barents Sea, by emplacement of dykes and sills (Corfu *et al.* 2013; Polteau *et al.* 2016; Minakov *et al.* 2018).

The Uralian orogeny (Early Carboniferous–Early Permian) associated with the closure of the Uralian Ocean (Churkin *et al.* 1981), is documented by Palaeozoic folding and thrusting with associated magmatism in the Polar Urals and on Taimyr (Faleide *et al.* 2018; and references therein). The later (Late Triassic–Early Jurassic) up-thrusting of Novaya Zemlya also partially affected Taimyr. These events mostly affected the eastern Barents Sea, which is reflected by the structural geometries of the East Barents

Basin. However, the main subsidence of the East Barents Basin was in late Permian–early Triassic times, thus post-dating the main Uralian event and pre-dating the younger Novaya Zemlya up-thrusting (Faleide *et al.* 2018).

Final continental breakup and onset of sea floor spreading in the NE Atlantic and the Arctic Eurasia Basin occurred around the Palaeocene–Eocene transition (Faleide *et al.* 2008; Minakov *et al.* 2012). A major shear system along the western Barents Sea–Svalbard margin linked the two spreading systems. The late Cenozoic uneven uplift of the entire Barents shelf triggered strong erosion, removing 1000–3000 m of sedimentary strata (Dimakis *et al.* 1998; Anell *et al.* 2009; Henriksen *et al.* 2011).

3 DATA AND MODELLING

The study is based on the wide-angle OBS data acquired in 2014. The data was acquired along a *ca.* 660-km-long NW–SE striking profile in the western Barents Sea. 38 OBS records are available, complimented by the onboard gravity, magnetic and sub-bottom profiler data. In addition, deep seismic reflection data acquired in 1985 [IKU-H line; (Gudlaugsson *et al.* 1987)], collocated with the OBS profile is used (Fig. 1). The technical details on the data acquisition and pre-processing of the 2014 data set are described in Aarseth *et al.* (2017). This study is based on the joint interpretation of the results of the seismic tomography (both *Vp* and *Vs*), depth migrated MCS data and gravity modelling.

3.1 Seismic tomography (*Vp*, *Vs*, *Vp*/*Vs* ratio)

The seismic modelling of the OBS data was performed using the joint refraction/reflection traveltime tomography code Tomo2D (Korenaga *et al.* 2000). The modelling was done independently for *Vp* and *Vs* models. The refracted and reflected traveltimes were manually picked for all major seismic phases. *P* phases were picked from hydrophone and vertical OBS component and *S* phases from horizontal components. The final data set for the *Vp* modelling consists of *ca.* 40 000 refracted traveltime picks (including Pg and Pn phases) and *ca.* 64 000 reflected traveltime picks from eight crustal interfaces (these include 3 intrasedimentary interfaces, top of the crystalline basement, 3 mid-crustal boundaries and the Moho reflection). Pick uncertainties were assigned to each pick, depending on the data quality (ranging from 25 ms for near offset refractions, to 90 ms for the weak secondary reflections). Example of the seismic section is shown in Fig. 2. For the *Vs* modelling the data set consists of *ca.* 15 400 refracted traveltime picks and 7500 Moho reflection picks. Reflections from other interfaces were difficult to identify, so they were omitted from modelling.

For the seismic modelling we took as a starting point the previous study of Aarseth *et al.* (2017). We used their reported forward modelled *Vp* velocity model as a starting model for the tomography inversion. For the shallow sedimentary layers we used the velocity information obtained from the velocity analysis of the collocated MCS line (see Section 3.3 for details). During the tomographic inversion we used the joint top-to-bottom and Monte Carlo modelling approach (for details see Shulgin *et al.* 2018). We inverted for the velocity and the geometry of the reflector for each layer, starting from the shallowest and then keeping it fixed, while modelling for deeper layers. For each layer the Monte Carlo modelling approach was used, building 20 semi-random starting conditions for the individual inversion. The modelling was done on a 2-D irregular grid, having a constant 500 m horizontal spacing, and vertically varying
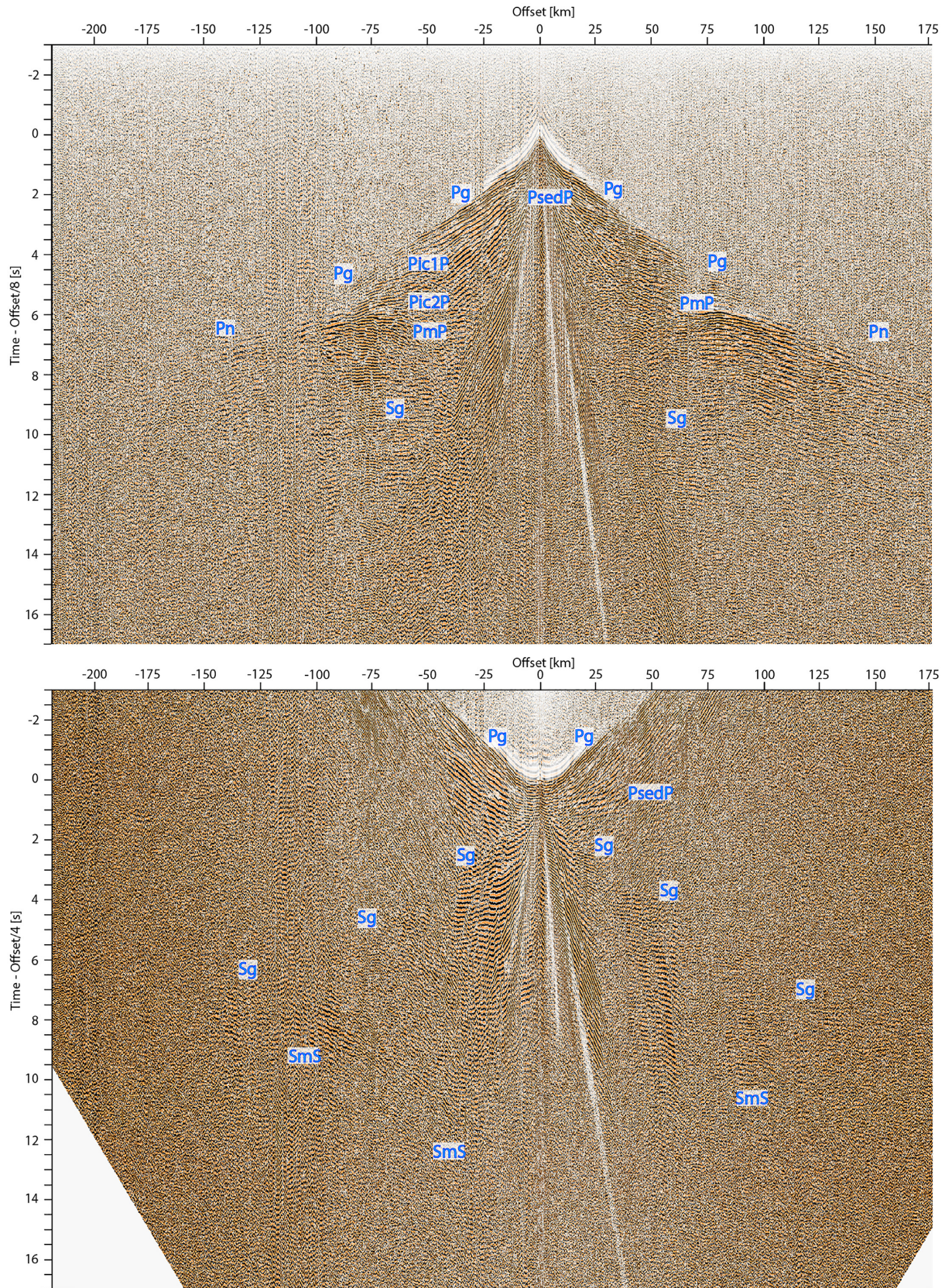
Figure 2. Example of seismic data section from OBS 227. Top panel: plotted with a reduction velocity of 8 km s^{-1} (to emphasize *P* phases). Bottom panel: same data plotted with a reduction velocity of 4 km s^{-1} (to emphasize *S* phases). P phases: Pg—crustal refraction, Pn—mantle refraction, PsedP—mid-sediments reflection, Pic1P and Pic2P—mid-crustal reflections, PmP—Moho reflection. S phases: Sg—crustal refraction, SmS—Moho reflection. For more data examples please see Aarseth *et al.* (2017).
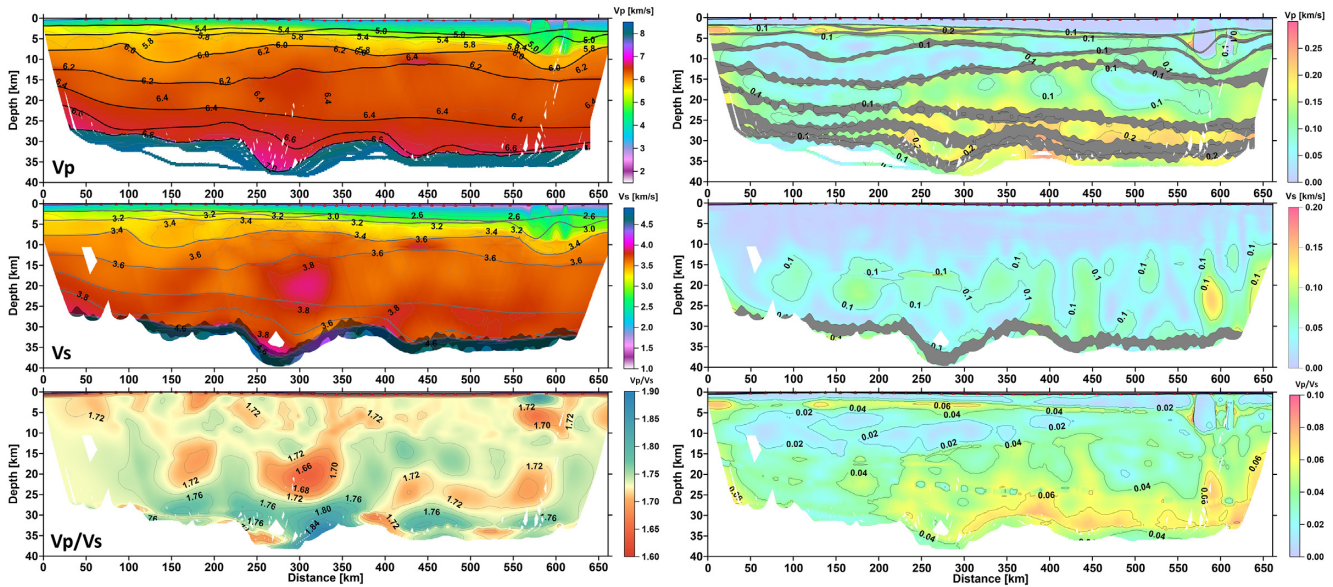
Figure 3. Tomography modelling results. Left-hand column shows the final velocity models and the best-fitting geometry of the reflectors in the crust. Right-hand column shows the errors of velocity modelling (background colour) and the uncertainties in the reflectors geometries (shaded areas). Top row: *Vp* modelling. Middle row: *Vs* modelling (only the Moho geometry is modelled with *S* waves; other interfaces are from *Vp* modelling—shown for reference). Bottom row: *Vp/Vs* ratio, based on the results of *Vp* and *Vs* models.

grid spacing ranging from 50 m at the surface and linearly increasing to 250 m at 50 km depth.

The starting velocity model (adapted from Aarseth *et al.* (2017)) was randomly 2-D perturbed with a ±10 per cent anomaly. Similarly, for each reflector the geometry at each node was randomly perturbed within ±15 per cent depth range. In addition, traveltime picks for each run were individually perturbed within the corresponding pick uncertainty. Combination of the perturbed starting velocity model, initial geometry of the reflector and modified traveltimes formed the basis for 20 tomographic inversions for each layer. A Monte Carlo statistical approach was used to estimate average resulting model/interface geometry and the modelling errors. The same approach was applied for both *Vp* and *Vs* modelling. The resulting final tomography models and the geometry of the interfaces are shown in Fig. 3.

The comparison of the tomography model with the forward model (Aarseth *et al.* 2017) shows in general similar features of the crustal structure, especially if compared in the depth domain. However, when the models are converted to the two-way-time (TWT) domain (Fig. 4), where the small variations in the velocities are emphasized, variations in Moho depth of *ca.* 1 s are observed. In fact, the observed misfit of the Moho position between the OBS forward model and the reflection data, triggered this study to apply different techniques and to reprocess both OBS and MCS data in order to investigate the observed mismatch.

3.2 Gravity modelling

Forward gravity modelling was performed to check the consistency of the final tomography models to the observed gravity anomaly data. We used shipborne gravity observations acquired along the profile during the OBS seismic experiment. For details on the gravity data acquisition and pre-processing, see Aarseth *et al.* (2017).

The gravity modelling was performed using the Oasis Montaj GM-SYS software. The geometry of the model was adopted from the results of the tomography modelling. The main goal of the gravity modelling was to check whether the densities converted from the velocities from the calculated tomography model fit the observed gravity field. For the initial gravity model the *Vp* velocities were converted to densities using empirical relationships for sediments and crystalline crust (Carlson & Herrick 1990; Christensen & Mooney 1995). The density of the lithospheric mantle and asthenosphere were kept fixed during modelling, with the corresponding values of 3340 and 3200 kg m^{-3}, respectively. During the modelling the geometry of the crustal interfaces was fixed, and we only varied local density values to obtain the best fit. In general, the crustal model derived from the seismic data, shows excellent fit in the gravity modelling, except at a few locations (Fig. 4). The gravity model requires the presence of a small high-density (*ca.* 2830 kg m^{-3}) body at the location of the 'Mjølnir' impact crater (Dypvik *et al.* 1996; Tsikalas *et al.* 2010), which is identified from the collocated MCS line, but too small to be confidently resolved by the wide-angle seismic data. The crust below the Nordkapp Basin (*ca.* 600 km profile distance) appears to be heavier and has shallower Moho, compared to the tomography predictions. This can be due to the presence of large salt diapirs close to the surface, as well as being located on the edge of the profile, resulting in limited number of seismic rays sampling the deep crustal structure below the basin.

3.3 MCS reprocessing

The seismic reflection line (IKU-H) collocated with the wide-angle profile was acquired in 1985. The interpretation of this data (Gudlaugsson *et al.* 1987; Ritzmann & Faleide 2007) revealed complex structuring of the basement along the line, with high reflectivity of the crust in the western (Caledonian) part, and almost non-reflective crust in the eastern (Timanian) domain. The locations of two sutures separating the crustal domains were proposed. However, due to limited length of the seismic streamer (3000 m) and the lack of deep-sampling seismic refraction profiles in the area, the velocity structure of the crystalline crust remained somewhat uncertain.
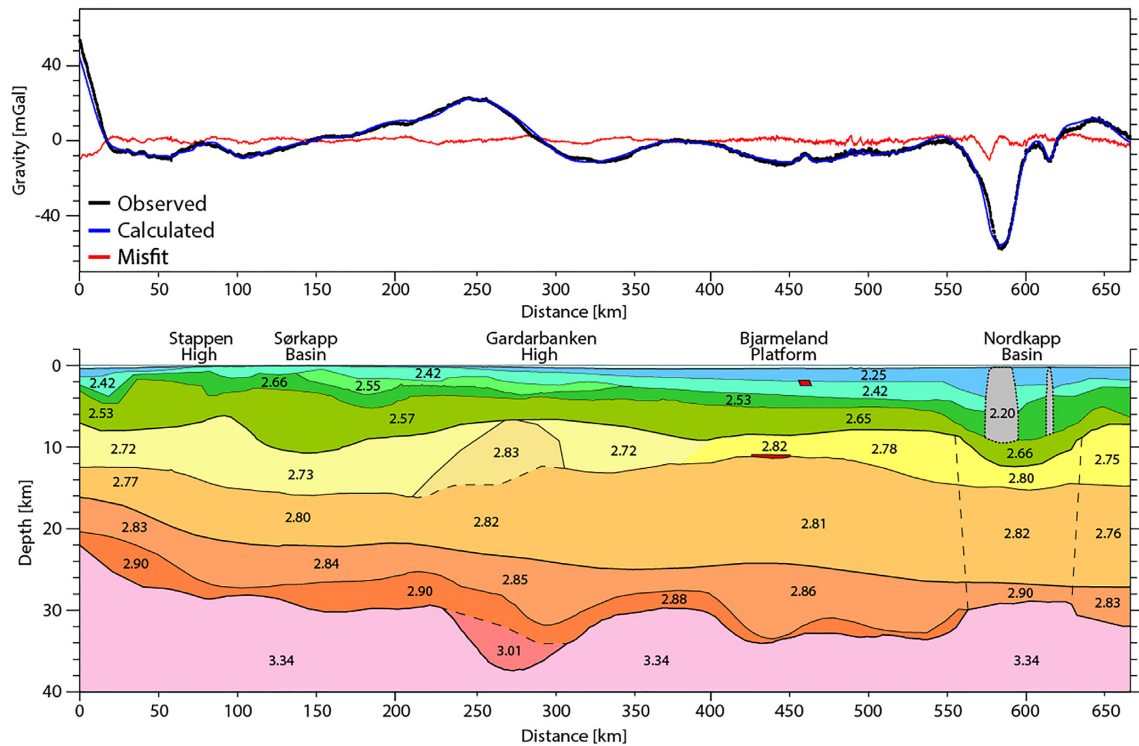
Figure 4. Gravity modelling results. Top panel: the observed (shipborne) and the calculated gravity anomalies along the profile. Bottom panel: density model, based on the results of seismic tomography. The shallow high-density anomaly (460 km) corresponds to the Mjølnir impact structure.

Furthermore, the original study of the IKU-H line (Ritzmann & Faleide 2007) is based on the depth conversion of the time-domain line drawing interpretation, but not the actual depth migration of the seismic data. The depth migration of the reflection data is dependent on the knowledge of the 2-D velocity distribution with depth, so the interpretation of the deep section was in question, also triggered by a comparison with the wide-angle forward model (Fig. 5).

We have reprocessed the original reflection data of 1985 utilizing the velocity model obtained in the tomography modelling using the RadexPro software. The processing was done using a conventional processing workflow, which included: geometry correction, source deconvolution, bandpass filtering, amplitude correction, multiple attenuation, stacking, and finally post-stack depth migration. For the velocity information, we have performed conventional velocity analysis of the reflection data for the shallow sedimentary strata (*ca.* down to 3 s) as it provides better resolution in the shallow portion of the model, compared to the wide-angle data. We further used this information in constraining the starting tomography models. For the deeper sections of the model the 2-D velocity field was taken from the *Vp* tomography model, constraining the seismic velocity for the entire model domain to the best possible resolution. The resulting PSDM seismic image is shown on Fig. 6. The use of the velocity distribution from the tomography model for the depth migration of the reflection data, allows for confident comparison of both results for joint interpretation in the depth domain.

4 RESULTS AND DISCUSSION

Fig. 7 summarizes the results of this study, including models of the *Vp*, *Vs*, *Vp*/*Vs* ratio, and density along the profile. These are compared to the reprocessed depth migrated MCS image along a major portion of the wide-angle profile.

The major differences in the present crustal model compared to the results of Aarseth *et al.* (2017) are related to the velocity values in the lower crust in the NW part of the profile (Fig. 4) as well as the geometry of the crustal root in the middle of the profile. The shallow (Carboniferous and younger sediments) portion of the profiles does not show significant changes. However, the updated/reprocessed tomography model provides more detailed image of lateral velocity variations. For the deeper crust, tomography model shows that the 'Caledonian' NW lower crust has velocities reaching 6.7 km s^{-1}, contrary to higher values of 6.9–7.0 km s^{-1} in Aarseth *et al.* (2017). The shape of the crustal root recovered from the tomography model also fits better with the collocated MCS results. As the MCS data have been reprocessed and depth migrated using the tomography velocity model—the results from tomography and MCS are directly comparable, which was a challenge previously. In their study of the IKU-H line, Ritzmann & Faleide (2007) utilized time-to-depth conversion of the line drawing interpretation, using only few 1-D velocity profiles along the transect.

In the following, we will describe and discuss the results addressing key features and questions related to the deep crustal-scale structure and evolution.

4.1 Reflectivity patterns

The analysis of the MCS data shows the principally different reflectivity patterns along the profile (Figs 6 and 7). The high reflectivity zone in the NW portion of the profile corresponds to the middle and lower crust on the Caledonian side, while there is basically no internal crystalline crustal reflectivity in the eastern part (within the Timanian basement). At the proposed location of the Caledonian termination zone (Fig. 8), we observe high crustal reflectivity, forming semi-horizontal and westward-dipping patterns, terminating at
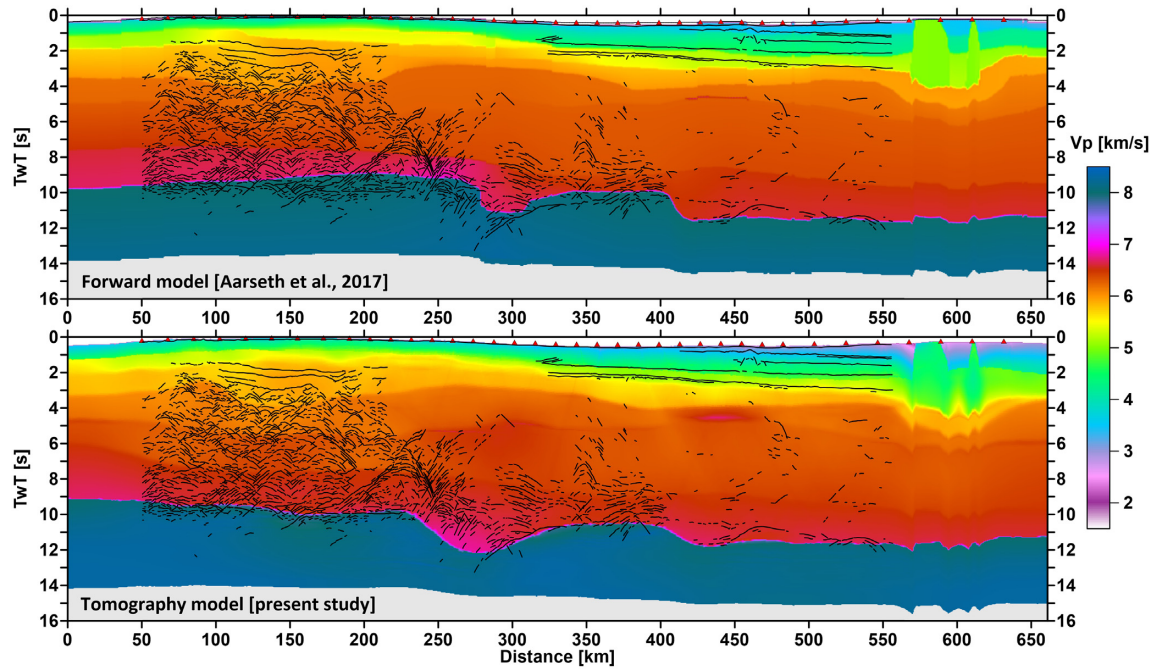
Figure 5. Comparison of the velocity structure along the profile. Top panel: forward model (Aarseth *et al.* 2017), bottom panel: tomography model (this study). Note, both models are converted from depth to two-way-traveltime and compared with the interpretation of the collocated reflection line (IKU-H) (Gudlaugsson *et al.* 1987; Ritzmann & Faleide 2007). Difference in the models are caused by using different modelling techniques and the number of traveltimes used in the modelling (*ca*. 5500 in forward modelling versus *ca*. 104 000 in the tomography).

Moho, with an abrupt decrease of reflectivity across the transition zone.

The observed reflectivity patterns resemble similar observations on the profile running across the Iapetus suture preceding the Caledonian orogeny west of Ireland (Klemperer 1989). Similarly to our profile, the predominantly subhorizontal or slightly dipping reflectivity patterns are observed in the middle-lower crust. The remnants of the suture are marked by a series of prominent lower crustal reflectors that are truncated at the Moho (on the Caledonian side), with significant decrease of crustal reflectivity on the other side of the suture zone. The crustal root that presumably was formed during the orogeny has been eliminated by post-orogenic extension and lower crustal ductile flow (Klemperer 1989). Mooney & Meissner (1992) inferred that the observed reflectivity is multigenetic in origin and is due to processes associated with both lithospheric collision and later extension.

The lack of crustal reflectivity in the eastern portion of the profile (in the Timanian domain) can be characteristic of relatively undeformed crust. The increase of lower crustal reflectivity in the western part can be caused by the emplacement of small amounts of fluids in microcracks and pores (Hyndman & Shearer 1989), or by emplacement of mafic sills, as there is apparent correlation between crustal reflectivity and high susceptibility magnetic blocks (Juhojuntti *et al.* 2001).

4.2 Moho geometry and crustal structure

Seismic tomography and gravity modelling reveal a complex Moho along the transect (Fig. 7). The NW portion of the profile shows an eastward dipping Moho from *ca*. 23 to 30 km over a distance of 100 km. The shallowing of the Moho to the west is expected, as the profile reaches the continent–ocean transition zone. Similar

Moho depth estimates were obtained on the neighbouring profile (Breivik *et al.* 2003, 2005). The *ca*. 150-km-long crustal segment below Stappen High and Sørkapp Basin (this study) shows a semi-flat Moho with small undulations, however the thickness of the crystalline crust changes from 22 to 17 km. This can represent the Caledonian nappes, cross-cut at low angle, and be similar to the interpreted structure of Profile 3 by Breivik *et al.* (2003, 2005).

The significant Moho deepening around Gardarbanken High is modelled by the tomography, gravity and is also visible in the reflection data. The dimensions of the crustal keel is *ca*. 70 km in width with the Moho depth increasing from 30 to about 37 km in the central part. The crustal root spatially correlates with the modelled zone of increased crustal *Vp* and densities. Similar observations have been previously reported for the nearby area around Loppa High (Clark *et al.* 2013). Furthermore, the modelled *Vp/Vs* ratio shows a well pronounced mid-crustal region of decreased values in the same location. The origin of this body will be discussed below.

The crustal structure below the Bjarmeland Platform (450–550 km profile distance) is rather homogeneous, with no significant lateral variations in the velocities or geometries of the crustal interfaces. The observed crustal structure is similar to the other profiles in the area located on the Timanian basement in the platform settings (Ivanova *et al.* 2011; Shulgin *et al.* 2018). This suggests that the observed structure can be characteristic for the relatively undeformed Timanian basement.

The SE part of the profile crosses the Nordkapp Basin, characterized by >10 km of sedimentary rocks and salt diapirs, which makes seismic modelling of the deep structures below it challenging. The tomography results show a semi flat Moho at a depth of 32–34 km, with an uncertainty of ±1–1.5 km. The crystalline crustal velocity structure is not showing any significant lateral variations. However, the gravity modelling requires increased densities in the middle/lower crust and a Moho shallowing of 4–5 km. The discrepancy
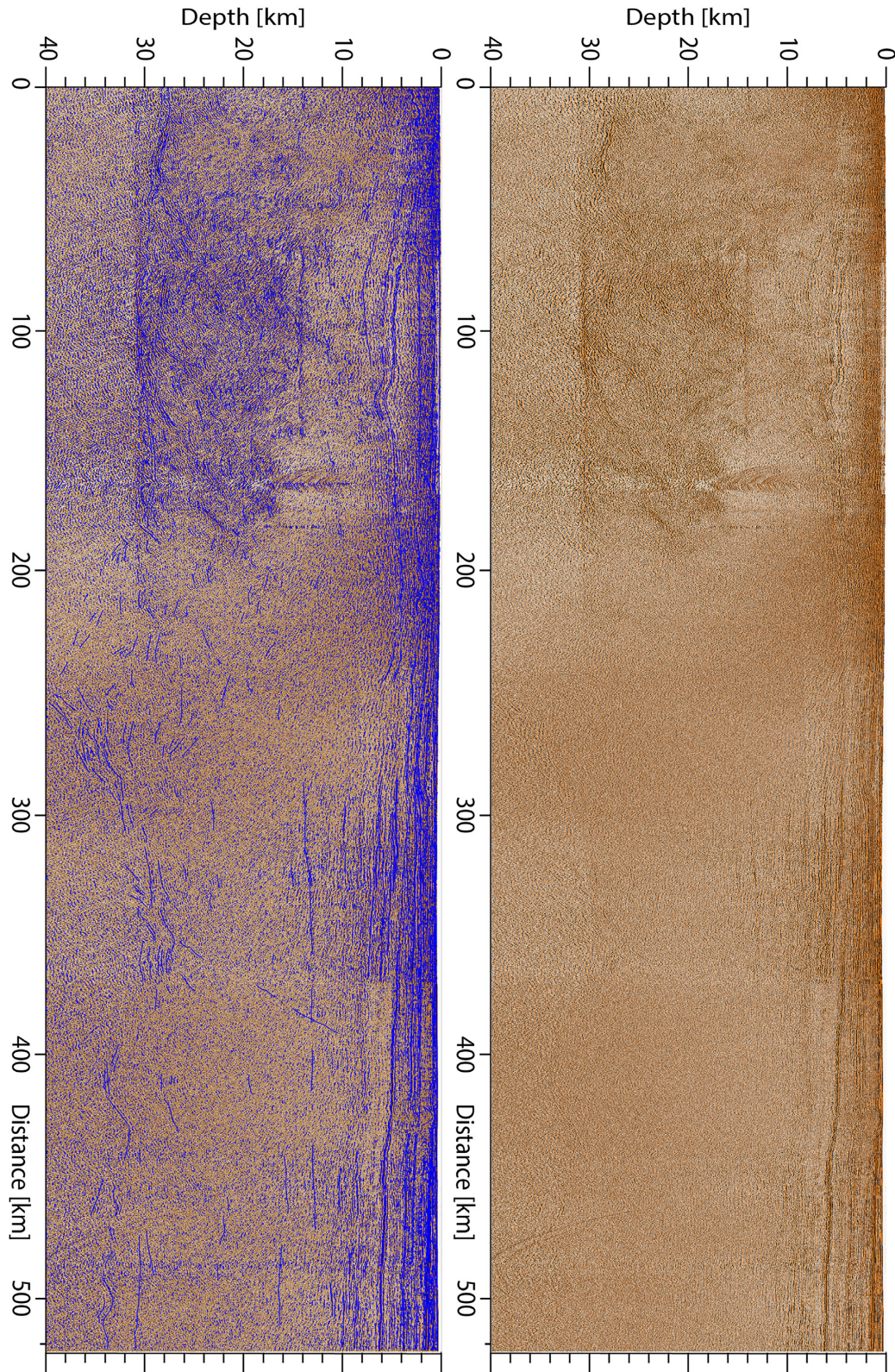
Figure 6. Post-stack depth migration of the reflection line IKU-H. on the bottom panel: blue lines show the simple line drawing interpretation of the seismic section. The lateral extent of the line is shown on Figs 1 and 4.
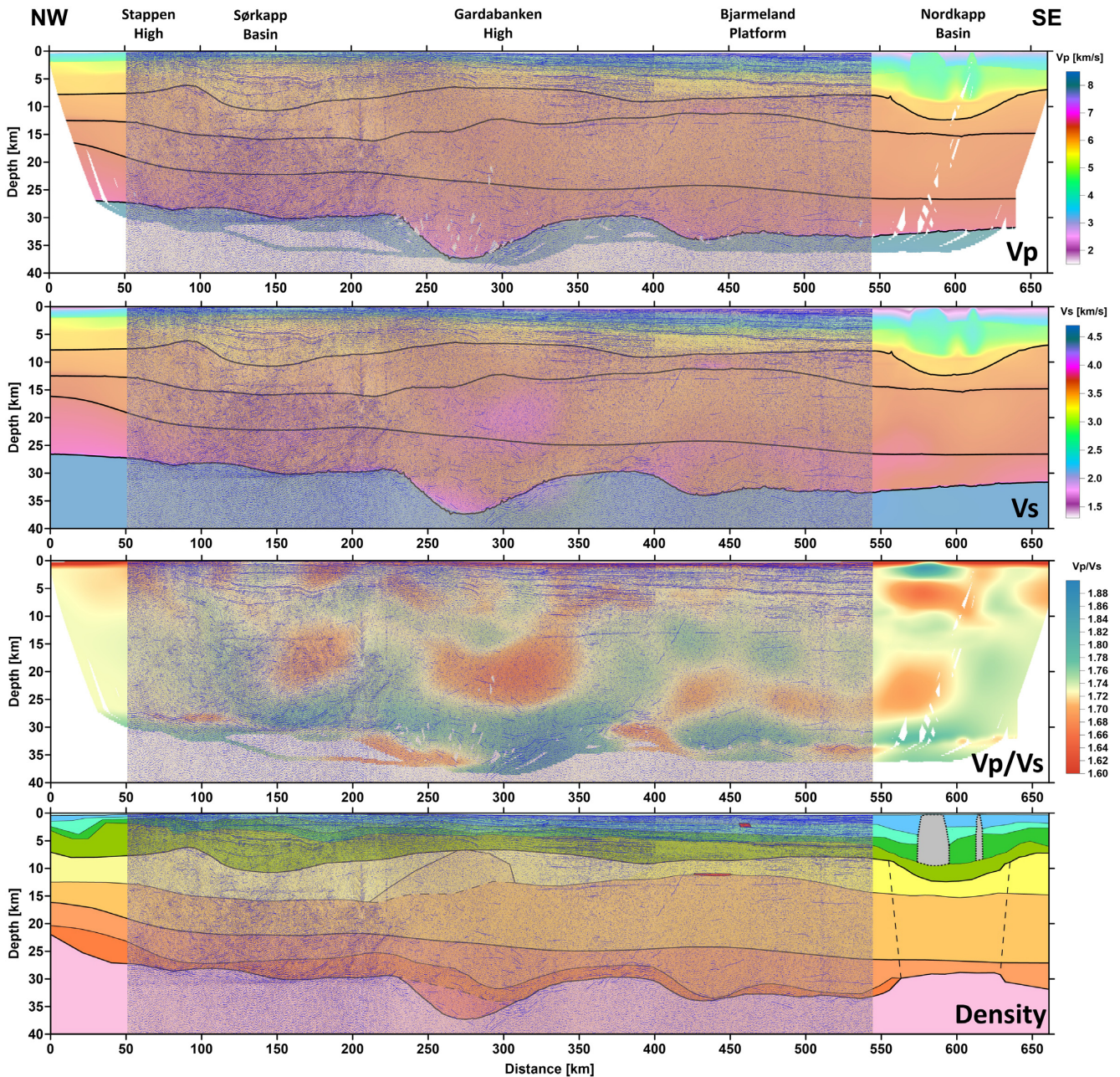
Figure 7. Summary of the modelling results. The panels (top to bottom): *Vp* model, *Vs* model, *Vp/Vs* ratio, density. The overlay on each plot is the simplified line drawing of the PSDM image of the reprocessed IKU-H data, emphasizing the reflectivity patterns.

between the seismic and gravity modelling is presumably caused by uncertainties in the seismic modelling due to the presence of large salt bodies close to the surface. We assume that the results from the gravity modelling are reliable, as the same basin shows similar crustal signature further southwest (Clark *et al.* 2013). Similar features have been reported for other rift related basins worldwide: Moho shallowing and mafic intrusions in the lower crust, resulting in increased densities (Thybo & Artemieva 2013).

4.3 Caledonian thrusts—suture zone?

We have looked on the 3-D crustal structure around the Sørkapp Basin and Gardarbanken High based on the seismic models of the OBS profiles in the area [Profiles 1–3 (Breivik *et al.* 2005), and this

study]. The idea was to constrain the Caledonian nappes surface (Breivik *et al.* 2005) onto our profile—effectively making it in a 3-D geometry. The lateral velocity changes and the undulations of the Moho and mid-crustal interfaces, as well as the crustal reflectivity patterns were taken into account. The proposed Caledonian–Timanian major thrust from Profile 3 of Breivik *et al.* (2005) was taken as a reference.

A plane surface was fitted to cross-cut 4 OBS profiles to delineate the possible western Caledonian suture branch in 3-D (Fig. 8). The projection of this cutting plane on the current profile is shown in Fig. 8. The cutting plane extends from the top of the interpreted location of the high-velocity/density body, and reaches the top of the crystalline basement under the Gardarbanken High. We should note that the proposed plane should be considered as a broad zone
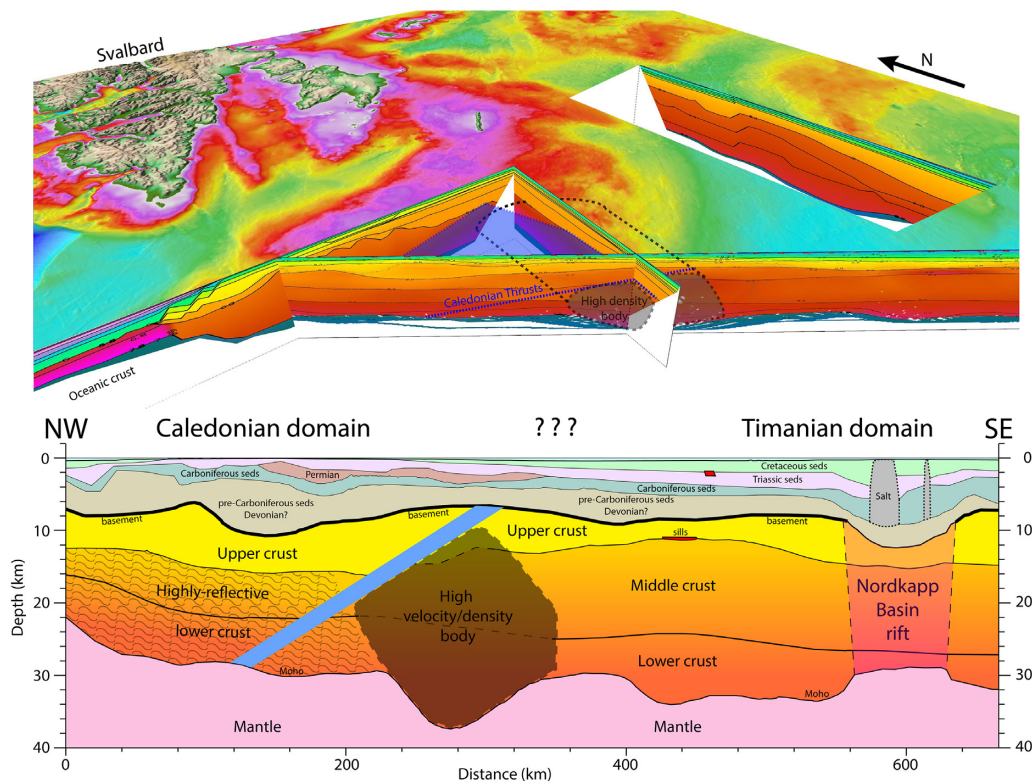
Figure 8. Top panel: 3-D view on the crustal cross-sections along the BarPz-P2 and Profile 3. The top plane shows the bathymetry. Blue cutting plane is the proposed Caledonian thrust in the area constrained by the 3-D analysis of the adjacent seismic profiles 1–3 (Breivik *et al.* 2005). The grey cylinder represents the high velocity/density body and its striking direction as identified from the profiles 4–7 (Breivik *et al.* 2002) and the BarPz-P2 profile. Bottom panel: schematic interpretation of the crustal architecture along the profile.

of the Caledonian—Timanian contact, rather than an actual fault plane. The wide-angle data, unfortunately, do not provide sufficient resolution to pinpoint the precise location, width and geometry of the suture, but rather provides the transition zone between these two crustal domains.

The projection of this plane on top of the regional map of crystalline basement (Klitzke *et al.* 2015) is shown by the blue line on Fig. 9. In the area where the plane is constrained by the seismic data there is a striking spatial correlation with the regional magnetic data (Gernigon & Brönner 2012), which indicate the eastward extent of the Caledonian terrane. The rocks forming the Caledonian nappes in the area are more magnetic compared to the Timanian crust, so when a certain thickness of the Caledonian nappes is reached, the aeromagnetic data reveals these lineaments (Gernigon & Brönner 2012).

Based on the Moho geometry and the lateral crustal variations of the velocities and *Vp/Vs* ratio we speculate that the proposed other suture (S3) by Ritzmann & Faleide (2007) (*ca.* 410 km profile distance) for the IKU-H reflection line can correspond to the same feature discussed above. The dashed blue line in Fig. 9 may be the extent of the Caledonian domain in the central Barents, with a step-like transition, rather than a gentle rotation as suggested by magnetic data (Gernigon & Brönner 2012). This follows the idea of Klitzke *et al.* (2019) suggesting that there is a pre-Caledonian rigid crustal block below the present day Sørkapp and Olga basins, which acted as a local barrier during the Caledonian orogeny, thus affecting the configuration of the Iapetus Ocean closure.

Alternatively, following the proposed ideas for a second branch of the 'Caledonian' suture, (Gudlaugson *et al.* 1998; Breivik *et al.* 2002, 2003, 2005; Aarseth *et al.* 2017) the Moho deepening (at

ca. 410 km profile distance) would correspond to a suture dipping towards SE and bounding the high-velocity/density body from the east. However, this suture must be pre-Caledonian, and be part of the Timanian terrane assemblage (Klitzke *et al.* 2019) and not been active since then, as it cuts the E–W oriented Olga Basin, where no N–S trending structures are observed.

4.4 High velocity/density body

An anomalous high-velocity/density crustal body identified from the tomography and gravity model is located in the middle part of the profile below the Gardabanken High. We address the origin of this anomalous body, as its density is significantly higher, compared to the adjacent upper crust. The decrease of the *Vp/Vs* ratio also characterizes the middle crust in this region, while both *Vp* and *Vs* are increased compared to adjacent areas (by 0.2 and 0.3 km s^{-1}, respectfully). The region is *ca.* 100–150 km wide and is affecting the upper, middle, and lower crust. The deep crustal root with the Moho deepening of 7–10 km is most likely associated with this anomalous body. The high densities identified at the bottom of this root, may suggest that the anomalous body extends from the top basement to the Moho. Based on the analysis of the possible Caledonian–Timanian contact zone location, it seems that the anomalous body is bounded by the proposed contact zone from the west and from the top (Fig. 8).

Comparison of the modelled properties of this anomalous body (*Vp*, *Vs*, density and *Vp/Vs* ratio) with the published data on different crystalline crustal rocks (Holbrook *et al.* 1992; Rudnick & Fountain 1995) is shown in Fig. 10. We have separated rock types into two
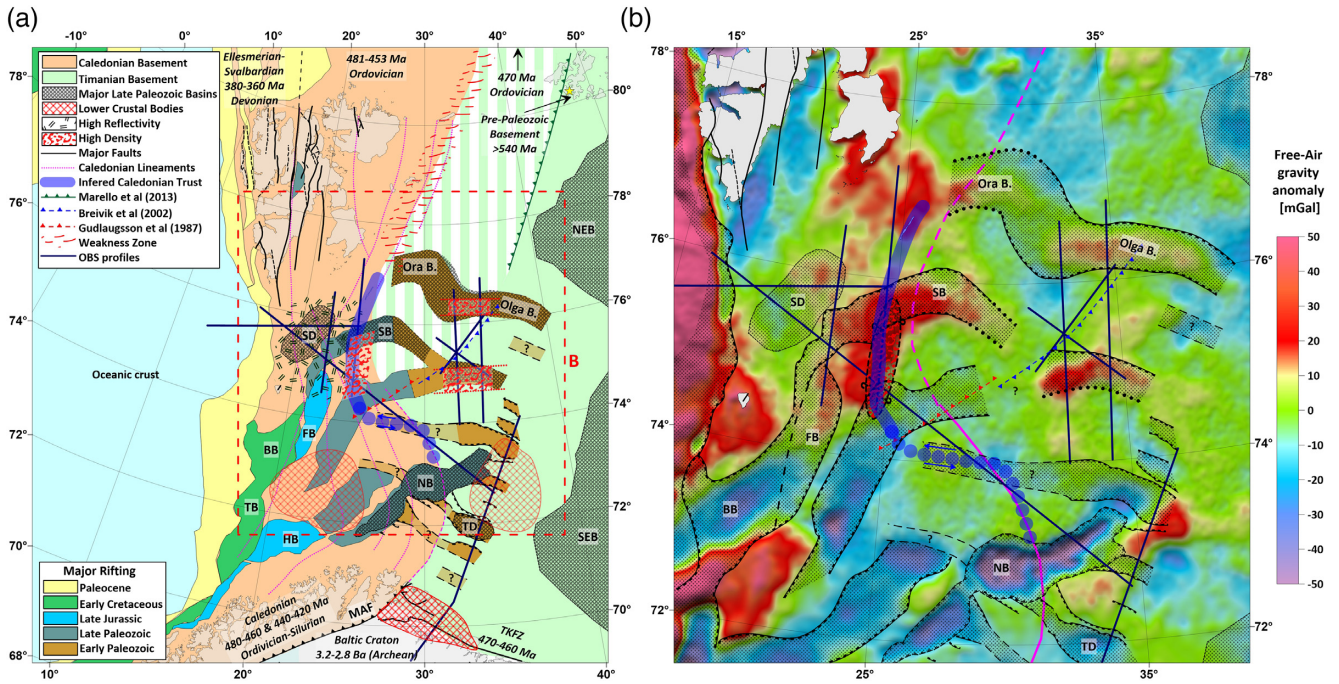
Figure 9. (a) Tectonic domains in the Western Barents Sea and major findings of this study. The locations of the wide-angle profiles are shown by black lines. The grey shading—major basins in the area. The Caledonian lineaments associated with magnetic basement highs (after Gernigon & Brönner 2012; Gernigon *et al.* 2014, 2018) are marked with purple lines. Shown ages refer to the age of the basement. Blue line (inferred Caledonian Trust) is the projection of the plane from Fig. 8 on the top of basement. The system of major rifts is modified after Faleide *et al.* (2008); rifts, graben, and half-grabens around eastern termination of the Nordkapp Basin are after Hassaan *et al.* (2020). The identified high-velocity/density crustal bodies (violet shading) correspond to the possible magmatic intrusions in the rifted basins. The anomalous lower crustal bodies are after Clark *et al.* (2013) and Shulgin *et al.* (2018). Red stippled box shows the extend of figure B. (b) Free-air gravity anomaly map ("DTU 2010"). The approximate extend of major basins is shown by shading. (BB)—Bjørnøya Basin; (GH)—Gardarbanken High; (HB)—Hammerfest Basin; (MAF)—Middle Allochthon Front; (NB)—Nordkapp Basin; (NEB)—Northeast Barents Basin; (Ori B.)—Ori Basin; (SB)—Sørvestsnaget Basin; (SD)—Sørkapp Depression; (SEH)—Sentralbanken High; (SEB)—Southeast Barents Basin; (TD)—Tiddlybanken Basin; (TKFZ)—Trollfjorden-Komagelva Fault Zone; (TB)—Tromsø Basin.

groups, representative for the upper-middle and lower crust. For the mid-crustal level the modelled properties of the anomalous body (Vp: 6.4–6.5 km s^{-1}; Vs: 3.7–3.8 km s^{-1}; density: 2830 kg m^{-3}) fall within the range of values typical for greenschists. For the lower crust level (Vp: 6.5–6.8 km s^{-1}; Vs: 3.6–3.8 km s^{-1}; density: 2870–3000 kg m^{-3}) it corresponds to mafic granulites.

The modelled properties of the anomalous body correspond to low-pressure low-moderate temperature metamorphic rocks, commonly associated with orogenesis. Based on this, two scenarios of the origin of this body arise. It may have originated from the mafic emplacement during the Neoproterozoic Timanian accretion, along the boundaries of a trapped crustal fragment, similar to the Olga crustal block (Klitzke *et al.* 2019); which was later metamorphosed during the main phase of the Caledonian orogeny. The observation, that the body is bounded from the top and from the west by the proposed extent of the Caledonian thrusts, supports this hypothesis (Fig. 8). In addition, such hypothesis can explain the reasoning for the 'eastern arm' of the Caledonian suture, discussed by Gudlaugsson *et al.* (1987), Breivik *et al.* (2002) and Marello *et al.* (2013). It is possible that what those authors interpreted as a suture, may be a linear westward dipping belt following the micro blocks boundaries of Timanian accretion, which were metamorphosed during the Caledonian, and thus exhibiting anomalous acoustic properties.

An alternative scenario is based on the comparison with similar identified high-velocity/density bodies on the OBS profiles to the east (Breivik *et al.* 2002), implying that the crustal body identified

on our profile can be linked to the southern anomalous body on the Breivik *et al.* (2002) profiles. If these bodies form a linear system striking in the W–E direction, this does not fit the Caledonian trend(s). The recent studies of the Olga Basin and surrounding area (Klitzke *et al.* 2019) suggested that the identified anomalous crustal bodies reported by Breivik *et al.* (2002) spatially coincide with the Olga Basin and a half-graben basin south of it. Klitzke *et al.* (2019) interpreted these bodies as magmatic intrusions during the rifting episode, which originally started in mid Devonian in the Pechora Basin and may have reached the central-northern Barents Sea by late Devonian–early Carboniferous, reactivating inherited Timanian weaknesses zones. This also coincides with the extensional collapse of the Caledonides, responsible for basin formation in the western Barents, and rifting on Svalbard (Gernigon *et al.* 2014; Klitzke *et al.* 2019). If the anomalous body identified on our profile is of the same origin (based on spatial correlations), this would imply that it also originated in late Devonian–Early Carboniferous along the existing pre-Caledonian structural weakness zone. This interpretation fits the geometrical considerations of the Palaeozoic rift systems in the western Barents Sea (Fig. 9). The W–E weakness zone associated with the Timanian accretion of the crustal fragments links to the NNE–SSW Palaeozoic rift system in the Caledonian domain in the central Barents Sea (Faleide *et al.* 2008). Thus, Carboniferous rifting along the inherited weakness zone converged to the present day location of the mafic intrusion, where the rifting direction changed. The change in the rifting direction can also be observed around the
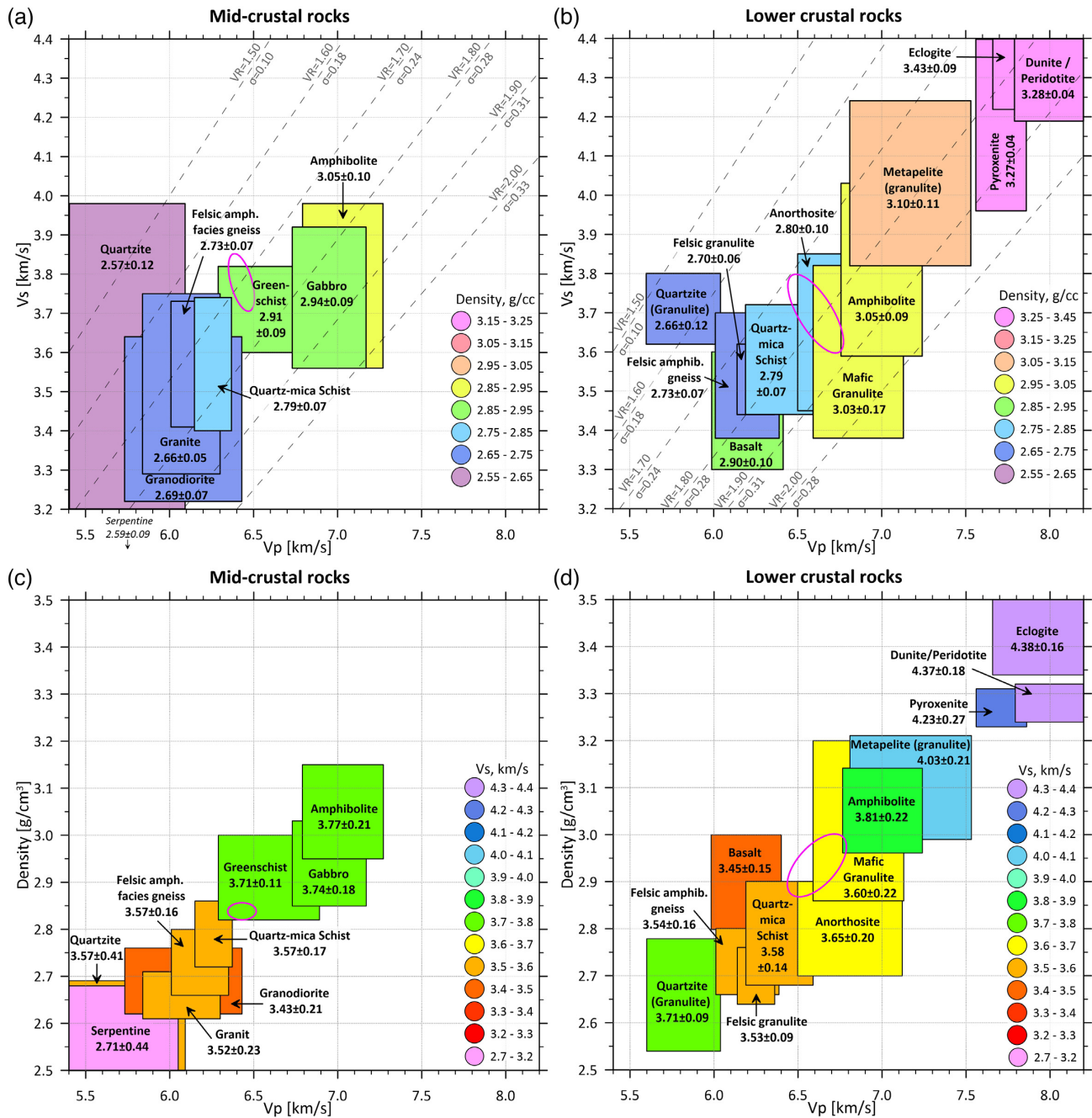
Figure 10. Comparison of the geophysical properties (*Vp*, *Vs*, density) of the major crustal rocks, based on Holbrook *et al.* (1992) and Rudnic & Fountain (1995). Panels (a) and (b) distribution of crustal rock properties in the *Vp–Vs* space for mid-crustal and lower crustal rocks, respectively. The colour-coding represents the densities of these rocks (also shown with numbers for the corresponding box). Grey stippled lines show isolines of constant *Vp/Vs* ration (VR) and constant Poisson ratio (σ). Panels (c) and (d) same data plotted in the *Vp*-density space. Colours and values correspond to the *Vs* values. Magenta ellipses denote modelled values of the high velocity/density body at mid and lower crustal levels, respectively.

SE part of the profile, where the NW–SE faults of the Timanian trend predates the NE–SW faults of the Nordkapp Basin (Hassaan *et al.* 2020).

4.5 Emplacement of sills

Emplaced sills have been observed in two locations along the profile: within the sedimentary fill of the Sørkapp Basin (Aarseth *et al.* 2017), and an intracrustal sill complex below the Bjarmeland Platform. The sills in the Sørkapp Basin are emplaced within the

sedimentary fill, which provides some stratigraphic age constraints (maximum age, as sills can be younger than the strata they are found in). The formation of the High Arctic LIP and the associated magmatism, including dyke swarms, occurred in the Early Cretaceous (Corfu *et al.* 2013; Polteau *et al.* 2016; Minakov *et al.* 2018). It is likely that the formation of the sills is directly associated with the LIP magmatism, either along faults generated during the rifting episode, or via reactivated Caledonian thrust faults. In addition, development of dykes feeding the sill complex below the Sørkapp Basin (Minakov *et al.* 2018) can also contribute to the increased

seismic reflectivity of the lower crust in this crustal domain. As an alternative, due to limited seismic resolution, the zones of increased velocities (up to 6.1 km s^{-1} within the sediments) could correspond to the thick carbonate platform developed in Upper Permian.

The intracrustal high-velocity layer (inferred from the refracted phases, implying a minimal thickness of *ca*. 200 m) identified below the Bjarmeland Platform (∼450 km profile distance) is interpreted as another sill complex. As it is not located within the sedimentary succession, the age constraints and its origin are very speculative. Spatially it correlates to the eastern extent of the Caledonian nappes, identified from the magnetic data (Gernigon *et al*. 2014, 2018). It also correlates with our proposed offset along the 'Olga' crustal block, corresponding to the Moho step, below the sill location. In both scenarios, the generation of sills seems to link to the edge of the Caledonian nappes, possibly fed via a weakness zone associated with the Caledonian thrusts. The age of the sill is unknown, but presumably corresponds to one of the known magmatic episodes: it may have formed in Late Devonian–early Carboniferous, associated with the magmatism developed during Pechora basin rifting, which propagated all the way to the central Barents Sea, analogues to the magmatism below Fedynsky High (Shulgin *et al.* 2018); or it can be associated with Early Cretaceous formation of the High Arctic LIP (Buchan & Ernst 2006), if it reached this area.

4.6 Basement origin between Timanian and Caledonian?

The area between Svalbard and Franz Josef Land, so called Barentsia (Gudlaugsson *et al.* 1987; Breivik *et al.* 2005) is still not fully understood due to lack of deep-sampling models (Fig. 9). However, the most recent studies of the reflection seismic data in the Olga and Sørkapp basins (Klitzke *et al.* 2019) suggest that this crustal domain should predate the Caledonian orogeny. This means that the proposed second Caledonian branch (Breivik *et al*. 2002, 2005), if it exists, is not Caledonian, but rather formed during the Neoproterozoic accretion of the Timanian terrane from crustal fragments. Most likely this western edge of the Timanian crust was assembled in the late Precambrian to Cambrian, prior to the closure of the Iapetus Ocean and initial stages of the Laurentia–Baltica collision. Such a fragment around the Gardarbanken High, carrying present-day Sørkapp and Olga basins, was proposed by Klitzke *et al.* (2019) and fits our interpretation. The presence of similar crustal fragments north of the Olga Basin is not clear. The area east of Svalbard is likely underlain by Caledonian basement, extending eastwards from Nordaustlandet (NE Svalbard) where Caledonian deformation is documented, and apparently can be extrapolated to the Lomonosov Ridge, based on the magnetic lineations (Knudsen *et al.* 2017). However, the presence of a parallel suture zone to the east, close to Franz Josef Land, has been suggested by Marello *et al.* (2013) based on gravity and magnetic data. This suggests the presence of another accreted pre-Caledonian crustal fragment between Svalbard and Franz Josef Land.

5 SUMMARY: DOMAINS AND TECTONIC EVOLUTION

We present an extended interpretation of the BarPz P2 wide-angle seismic profile, originally reported by Aarseth *et al.* (2017). The new results are based on tomographic modelling of *Vp*, *Vs*, *Vp/Vs* ratio, a reprocessed depth migrated collocated seismic reflection profile, and complimented by gravity modelling.

The major findings are:

(1) We document in 3-D the position of the Caledonian nappes in the western Barents Sea, which fits the proposed extent from regional aeromagnetic data.

(2) The Caledonian domain is characterized by high crustal reflectivity, caused by strong deformation and/or emplacement of mafic intrusions within the crystalline crust. The Timanian domain shows semi-transparent crust with little internal reflectivity, suggesting less deformation.

(3) The crustal domain in-between two proposed arms of the Caledonian suture represents pre-Caledonian crustal fragments accreted to the Timanian terrane, most likely in early Cambrian. This crustal block may have an E–W striking southern boundary, along which the Caledonian nappes were offset.

(4) A high-velocity/density crustal body, adjacent to the Caledonian–Timanian contact zone, is interpreted as a zone of distinct metamorphosed rocks different from the surrounding crust, based on the comparison with global compilations.

(5) Two scenarios for the origin of the body are proposed. First, mafic emplacement during the Timanian assembly, which was metamorphosed during the Caledonian orogeny, spatially correlated with the regional gravity maxima zone. Alternatively, massive mafic intrusions associated with Devonian rifting, which reactivated the inherited structures in both Timanian and Caledonian domains.

(6) Emplacement of mafic material in Late Devonian–Early Carboniferous into the crust under the Nordkapp Basin is speculatively inferred from the gravity modelling.

REFERENCES

Aarseth, I., Mjelde, R., Breivik, A.J., Minakov, A., Faleide, J.I., Flueh, E. & Huismans, R.S., 2017. Crustal structure and evolution of the Arctic Caledonides: Results from controlled-source seismology, *Tectonophysics,* **718,** 9–24.

Andersen, O. B., Knudsen, P. & Berry, P., 2010. The DNSC08GRA global marine gravity field from double retracked satellite altimetry, *Journal of Geodesy,* **84** (3) DOI: 10.1007/s00190-009-0355-9.

Anell, I., Thybo, H. & Artemieva, I.M., 2009. Cenozoic uplift and subsidence in the North Atlantic region: geological evidence revisited, *Tectonophysics,* **474,** 78–105.

Barrere, C., Ebbing, J. & Gernigon, L., 1999. Offshore prolongation of Caledonian structure and basement characterisation in the western Barents Sea from geophysical modelling, *Tectonophysics,* **470** (1), 71–88, doi:10.1016/j.tecto.2008.07.012.

Barrère, C., Ebbing, J. & Gernigon, L., 2011. 3-D density and magnetic crustal characterization of the southwestern Barents shelf: Implications for the offshore prolongation of the Norwegian Caledonides, *Geophys. J. Int.,* **184**(3), 1147–1166.

Bogdanov, N.A. & Hain, V.E., 1996. Tectonic map of the Barents Sea and northern part of European Russia, *Geol. Inst., Russ. Acad. Sci.,* 101 p., doi:10.13140/2.1.2476.0008.

Breivik, A.J., Mjelde, R., Grogan, P., Shimamura, H., Murai, Y. & Nishimura, Y., 2003. Crustal structure and transform margin development south of Svalbard based on ocean bottom seismometer data, *Tectonophysics,* **369**(1–2), 37–70.

Breivik, A.J., Mjelde, R., Grogan, P., Shimamura, H., Murai, Y. & Nishimura, Y., 2005. Caledonide development offshore-onshore Svalbard based on ocean bottom seismometer, conventional seismic, and potential field data, *Tectonophysics,* **401**(1–2), 79–117.

Breivik, A.J., Mjelde, R., Grogan, P., Shimamura, H., Murai, Y., Nishimura, Y. & Kuwano, A., 2002. A possible Caledonide arm through the Barents Sea imaged by OBS data, *Tectonophysics,* **355**(1–4), 67–97.

Buchan, K.L. & Ernst, R.E., 2006. *The High Arctic Large Igneous Province (HALIP): Evidence for an Associated Giant Radiating Dyke Swarm,* Large Igneous Provinces Commission.

Carlson, R.L. & Herrick, C.N., 1990. Densities and porosities in the oceanic crust and their variations with depth and age, *J. geophys. Res.,* **95**, 9153–9170.

Christensen, N.I. & Mooney, W.D., 1995. Seismic velocity structure and composition of the continental crust: a global view, *J. geophys. Res.,* **100**, 9761–9788.

Churkin, M. J., Soleimani, G., Carter, C. & Robinson, R., 1981, Geology of the Soviet Arctic: Kola Peninsula to Lena river. In *'The Ocean Basins and Margins, The Arctic Ocean",* Vol. 5, pp. 331–375, eds Nairn, A. E. M., Churkin, M. J. & Stehli, F. G., Plenum Press, New York.

Clark, S.A., Faleide, I.J., Hauser, J., Ritzmann, O., Mjelde, R., Ebbing, J., Thybo, H. & Flueh, E., 2013. Stochastic velocity inversion of seismic reflection/refraction traveltime data for rift structure of the southwest Barents Sea, *Tectonophysics,* **593**, 135–150.

Corfu, F., Polteau, S., Planke, S., Faleide, J., Svensen, H., Zayonchek, A. & Stolbov, N., 2013. U–Pb geochronology of Cretaceous magmatism on Svalbard and Franz Josef Land, Barents Sea Large Igneous Province, *Geol. Mag.,* **150**(6), 1127–1135.

Dimakis, P., Braathen, B.I., Faleide, J.I., Elverhoi, A. & Gudlaugsson, S.T., 1998. Cenozoic erosion and the preglacial uplift of the Svalbard-Barents Sea region, *Tectonophysics,* **300**(1–4), 311–327.

Doré, A.G., Lundin, E.R., Fichler, C. & Olesen, O., 1997. Patterns of basement structure and reactivation along the NE Atlantic margin, *J. Geol. Soc.,* **154**(1), 85–92.

Dypvik, H. *et al.*, 1996. Mjølnir structure: an impact crater in the Barents Sea, *Geology,* **24**(9), 779–782.

Faleide, J.I., Gudlaugsson, S.T. & Jacquart, G., 1984. Evolution of the western Barents Sea, *Mar. Pet. Geol.,* **1**(2), 123–150.

Faleide, J.I., Pease, V., Curtis, M., Klitzke, P., Minakov, A., Scheck-Wenderoth, M., Kostyuchenko, S. & Zayonchek, A., 2018. Tectonic implications of the lithosphere structure across the Barents and Kara shelves, in *Circum-Arctic Lithopheric Evolution,* p. 460, eds Pease, V. & Coakley, B., Geological Society, London Special Publications.

Faleide, J.I., Tsikalas, F., Breivik, A.J., Mjelde, R., Ritzmann, O., Engen, O., Wilson, J. & Eldholm, O., 2008. Structure and evolution of the continental margin off Norway and Barents Sea, *Episodes,* **31**(1), 82–91.

Faleide, J.I., Vagnes, E. & Gudlaugsson, S.T., 1993. Late Mesozoic-Cenozoic evolution of the southwestern Barents Sea in a regional rift shear tectonic setting, *Mar. Pet. Geol.,* **10**, 186–214.

Gee, D.G., Bogolepova, O.K. & Lorenz, H., 2006. The Timanide, Caledonide and Uralide orogens in the Eurasian high Arctic, and relationships to the paleo-continents Laurentia, Baltica and Siberia, *Geol. Soc., Lond., Memoirs,* **32**(1), 507–520.

Gee, D.G. & Pease, V., 2004. The Neoproterozoic Timanide Orogen of eastern Baltica: Introduction, *Geol. Soc., Lond., Memoirs,* **30**(1), 1–3.

Gernigon, L. & Brönner, M., 2012. Late Palaeozoic architecture and evolution of the southwestern Barents Sea: Insights from a new generation of aeromagnetic data, *J. Geol. Soc., London,* **169**(4), 449–459.

Gernigon, L., Brönner, M., Dumais, M.A., Gradmann, S., Grønlie, A., Nasuti, A. & Roberts, D., 2018. Basement inheritance and salt structures in the SE Barents Sea: insights from new potential field data, *J. Geodyn.,* **119**, 82–106.

Gernigon, L., Brönner, M., Roberts, D., Olesen, O., Nasuti, A. & Yamasaki, T., 2014. Crustal and basin evolution of the southwestern Barents Sea: From Caledonian orogeny to continental breakup, *Tectonics,* **33**, 347–373.

Gudlaugsson, S.T., Faleide, J.I., Fanavoll, S. & Johansen, B., 1987. Deep seismic reflection profiles across the western Barents Sea, *Geophys. J. R. astr. Soc.,* **89**, 273–278.

Gudlaugsson, S. T., Faleide, J. I., Johanses, S. E. & Breivik, A. J., 1998. Late Paleozoic structural development of the south western Barents Sea., *Marine and Petroleum Geology,* **15**, 73–102.

Hassaan, M., Faleide, J.I., Gabrielsen, R.H. & Tsikalas, F., 2020. Carboniferous graben structures, evaporite accumulations and tectonic inversion in southeastern Norwegian Barents Sea, *Mar. Petrol. Geol.,* **112**, doi:10.1016/j.marpetgeo.2019.104038.

Henriksen, E. *et al.*, 2011. Uplift and erosion of the greater Barents Sea: impact on prospectivity and petroleum systems, *Geol. Soc. Lond., Memoirs,* **35**(1), 271–281.

Holbrook, W.S., Mooney, W.D. & Christensen, N.I., 1992. The seismic velocity structure of the deep continental crust, in *Continental Lower Crust,* pp. 1–44, eds Fountain, D.M., Arculus, R. & Kay, R.W., Elsevier Sci.

Hyndman, R.D. & Shearer, P.M., 1989. Water in the lower continental crust: modelling magnetotelluric and seismic reflection results, *Geophys. J. Int.,* **98**, 343–365.

Ivanova, N.M., Sakulina, T.S., Belyaev, I.V., Matveev, Y.I. & Roslov, Y.V., 2011. Depth model of the Barents and Kara seas according to geophysical surveys results, in *Arctic Petroleum Geology,* Vol. 35, pp. 209–221, eds Spencer, A.M., Embry, A.F., Gautier, D.L., Stoupakova, A. & Sørensen, K., Geol. Soc., London, Memoirs.

Johansen, S.E., Henningsen, T., Rundhovde, E., Saether, B.M., Fichler, C. & Rueslatten, H.G., 1994. Continuation of the Caledonides North of Norway—seismic reflectors within the basement beneath the Southern Barents Sea, *Mar. Pet. Geol.,* **11**(2), 190–201.

Juhojuntti, N., Juhlin, C. & Dyrelius, D., 2001. Crustal reflectivity underneath the Central Scandinavian Caledonides, *Tectonophysics,* **224**(3-4), 191–210.

Klemperer, S.L., 1989. Seismic reflection evidence for the location of the Iapetus suture west of Ireland, *J. Geol. Soc., London,* **146**, 409–412.

Klitzke, P., Faleide, J.I., Schcke-Wenderoth, M. & Sippel, J., 2015. A lithosphere-scale structural model of the Barents Sea and Kara Sea region, *Solid Earth,* **6**, 153–172.

Klitzke, P., Franke, D., Ehrhardt, A., Lutz, R., Reinhardt, L., Heyde, I. & Faleide, J.I., 2019. The Paleozoic evolution of the Olga Basin region, northern Barents Sea: a link to the Timanian orogeny, *Geochem. Geophys. Geosyst.,* **20**, doi:10.1029/2018GC007814.

Knudsen, C. *et al.*, 2017. Samples from the Lomonosov ridge place new constraints on the geological evolution of the Arctic Ocean, *Geol. Soc., Lond., Spec. Publ.,* **460**(1), 397–418.

Korenaga, J., Holbrook, S., Kent, G., Kelemen, P., Detrick, R.S., Larsen, H.-C., Hopper, J.R. & Dahl-Jensen, T., 2000. Crustal structure of the southeast Greenland margin from joint refraction and reflection seismic tomography, *J. geophys. Res.,* **105**, 21 591–21 614.

Kostyuchenko, S., Sapozhnikov, R., Egorkin, A., Gee, D., Berzin, R. & Solodilov, L., 2006. Crustal structure and tectonic model of northeastern Baltica, based on deep seismic and potential field data, in *European Lithosphere Dynamics,* Vol. 32, pp. 521–539, eds Gee, D.G. & Stephenson, R.A., Geol. Soc., London, Memoirs.

Manby, G. & Lyberis, N., 1992. Tectonic evolution of the Devonian Basin of northern Svalbard, *Nor. Geol. Tidsskr.,* **72**(1), 7–19.

Marello, L., Ebbing, J. & Gernigon, L., 2013. Basement inhomogeneities and crustal setting in the Barents Sea from a combined 3-D gravity and magnetic model, *Geophys. J. Int.,* **193**, 557–584.

Minakov, A., Faleide, J.I., Glebovsky, V.Y. & Mjelde, R., 2012. The structure and evolution of the Northern Barents–Kara Sea continental margin from integrated analysis of potential field, bathymetry and sparse seismic data, *Geophys. J. Int.,* **188**, 79–102.

Minakov, A., Yarushina, V., Faleide, J.I., Krupnova, N., Sakoulina, T., Dergunov, N. & Glebovsky, V., 2018. Dyke emplacement and crustal structure within a continental large igneous province, northern Barents Sea, *Geol. Soc., Lond., Spec. Publ.,* **460**, 371–395.

Mooney, W.D. & Meissner, R., 1992. Multi-genetic origin of crustal reflectivity: a review of seismic reflection profiling of the continental lower crust and Moho, in *Continental Lower Crust,* 45–79, eds Fountain, D.M., Arculus, R. & Kay, R.W., Elsevier.

Pease, V., 2011. Chapter 20: Eurasian orogens and Arctic tectonics: an overview, *Geol. Soc., Lond., Memoirs,* **35**(1), 311–324.

Pease, V. & Scott, R.A., 2009. Crustal affinities in the Arctic Uralides, northern Russia: significance of detrital zircon ages from Neoproterozoic and Paleozoic sediments in Novaya Zemlya and Yaimir, *J. geol. Soc. Lond.,* **166**, 517–527.

Polteau, S. *et al.*, 2016. The early cretaceous Barents Sea sill complex: distribution, Ar/Ar geochronology and implications for carbon gas formation, *Palaeogeog. Palaeoclimat. Palaeoecol.,* **441**, 83–95.

Ritzmann, O. & Faleide, J.I., 2007. Caledonian basement of the western Barents Sea, *Tectonics,* **26**(5), doi:10.1029/2006TC002059.

Ritzmann, O. & Faleide, J.I., 2009. The crust and mantle lithosphere in the Barents Sea/Kara Sea region, *Tectonophysics,* **470**(1–2), 89–104.

Roberts, D., 2003. The Scandinavian Caledonides: event chronology, paleogeographic settings and likely modern analogues, *Tectonophys,* **365**, 289–299.

Roberts, D. & Siedlecka, A., 2002. Timanian orogenic deformation along the northeastern margin of Baltica, Northwest Russia and Northeast Norway, and Avalonian–Cadomian connections, *Tectonophysics,* **352**, 169–184.

Rudnick, R.L. & Fountain, D.M., 1995. Nature and composition of the continental crust: a lower crustal perspective, *Rev. Geophys.,* **33**(3), 267–309.

Shulgin, A., Mjelde, R., Faleide, J.I., Høy, T., Flueh, E. & Thybo, H., 2018. The crustal structure in the transition zone between the western and eastern Barents Sea, *Geophys. J. Int.,* **214**, 315–330.

Stoupakova, A.V. *et al.*, 2011. The geological evolution and hydrocarbon potential of the Barents and Kara shelves, *Geol. Soc., Lond., Memoirs,* **35**(1), 325–344.

Thybo, H. & Artemieva, I.M., 2013. Moho and magmatic underplating in continental lithosphere, *Tectonophysics,* **609**, doi:10.1016/j.tecto.2013.05.032.

Tsikalas, F., Dypvik, H. & Smelror, M., 2010. *The Mjølnir Impact Event and its Consequences,* Springer, doi:10.1007/978-3-540-88260-2.

Worsley, D., 2008. The post-Caledonian development of Svalbard and the western Barents Sea, *Polar Res.,* **27**(3), 298–317.

SUPPORTING INFORMATION

Supplementary data are available at *GJI* online.

Figure S1. Results of the tomographic modelling (top: *Vp*; bottom: *Vp*/*Vs*/ratio) converted from depth to two-way-traveltime. The overlay is the early line drawing interpretation of collocated reflection line IKU-H (Gudlaugsson *et al.* 1987; Ritzmann & Faleide 2007). The interpretation is in a good agreement with the tomography model, however the central part of the profile, where the transition from the Timanian to Caledonian domain is proposed, lacks details in the reflection data.

Please note: Oxford University Press is not responsible for the content or functionality of any supporting materials supplied by the authors. Any queries (other than missing material) should be directed to the corresponding author for the paper.